

# Cu $K$ -edge Resonant Inelastic X-Ray Scattering in Edge-Sharing Cuprates

F. Vernay<sup>1,2</sup>, B. Moritz<sup>1,2</sup>, I. S. Elfimov<sup>3</sup>, J. Geck<sup>3</sup>, D. Hawthorn<sup>3</sup>, T. P. Devereaux<sup>1,2</sup>, and G. A. Sawatzky<sup>2,3</sup>

<sup>1</sup> *Department of Physics and Astronomy, University of Waterloo, Waterloo, Ontario N2L 3G1, Canada*

<sup>2</sup> *Pacific Institute of Theoretical Physics, University of British Columbia, Vancouver BC and*

<sup>3</sup> *Department of Physics, University of British Columbia, Vancouver, BC*

(Dated: February 4, 2008)

We present calculations for resonant inelastic x-ray scattering (RIXS) in edge-shared copper oxide systems, such as  $\text{Li}_2\text{CuO}_2$  and  $\text{CuGeO}_3$ , appropriate for hard x-ray scattering such as the copper  $K$ -edge. We perform exact diagonalizations of the multi-band Hubbard model and determine the energies, orbital character and resonance profiles of excitations which can be probed via RIXS. We find excellent agreement with recent results on  $\text{Li}_2\text{CuO}_2$  and  $\text{CuGeO}_3$  in the 2-7 eV photon energy loss range.

PACS numbers: 78.70.Ck, 78.67-n, 78.20.Bh, 78.66.Nk

## I. INTRODUCTION

Techniques that probe the momentum dependence of strongly correlated electrons provide valuable information that can be used as a test for models appropriate for the cuprates. Angle-resolved photoemission (ARPES) provides important information about single-particle excitations of occupied states.<sup>1,2</sup> Electronic Raman scattering reveals information about multiparticle excitations at long wavelengths.<sup>3</sup> Resonant inelastic x-ray scattering (RIXS), a form of Raman spectroscopy, recently has undergone vast improvements, allowing probes of momentum dependent excitations into unoccupied states.<sup>4</sup> Improvements in resolution now offer the possibility of a direct comparison of ARPES, Raman, and RIXS spectra in the several eV range with the hope of understanding the nature of strong correlations in the cuprates, and high temperature superconductivity, by studying electronic excitations at several energy scales.

As a fundamental building block of low-energy effective theories of the cuprates, the Zhang-Rice singlet (ZRS)<sup>5</sup> is the starting point of the single-band Hubbard and t-J models widely believed to capture the low energy physics of strongly correlated systems. It is well-known that the ZRS features prominently in RIXS in the cuprates. A particular test of models of the cuprates lies in the difference between RIXS in edge-shared versus corner-shared copper oxide systems. In materials such as  $\text{La}_2\text{CuO}_4$  and other corner sharing 2D members of the high  $T_c$  family, the ZRS is stabilized by a strong gain in anti-ferromagnetic exchange energy between Cu and O, and can propagate to neighboring  $\text{CuO}_4$  plaquettes, with effective hopping  $t = -0.35$  eV along the Cu-O bond direction, and  $t' = 0.15$  eV along the diagonal.<sup>5</sup> In edge-shared cuprates, such as  $\text{Li}_2\text{CuO}_2$  and  $\text{CuGeO}_3$ , the Cu-O-Cu bond approximately forms a  $90^\circ$ -angle,<sup>6</sup> compared to  $180^\circ$  in corner-shared cuprates, and therefore according to Goodenough-Kanamori-Anderson,<sup>7</sup> the nearest-neighbor copper-copper exchange tends to be slightly ferromagnetic. However, higher order processes like Cu-O-O-Cu hopping also contribute comparable antiferromagnetic exchange terms. For these reasons, small bond-

angle variations among different edge-sharing compounds can make the exchange slightly anti-ferromagnetic or ferromagnetic. In either case, the ZRS is less stable and mobile due to hybridization among different oxygen orbitals not aligned with Cu  $d_{x^2-y^2}$  orbitals.<sup>6</sup>

Recent Cu  $K$ -edge RIXS data on edge-sharing cuprate  $\text{Li}_2\text{CuO}_2$ <sup>8,9</sup> has revealed a small, non-dispersive peak at 2.1 eV, attributed to interatomic  $d-d$  excitations, a strong peak at 5.4 eV, and a weak peak at 7.6 eV, both attributed to charge transfer excitations. The peak at 5.4 eV is doubly resonant for incident photon energies near 8986 and 9000 eV.<sup>8</sup> In  $\text{CuGeO}_3$ , clear excitations were found are 3.8 eV (weak) and 6 eV (strong),<sup>9,10,11</sup> and more recently 1.7 eV,<sup>12</sup> which were attributed in Ref. 12 as a intra-atomic  $d-d$  excitation (1.7 eV), a ZRS excitation (3.8 eV), and a charge transfer excitation on a single copper oxide plaquette (6.4 eV). Similar features have also appeared in oxygen 1s RIXS.<sup>13</sup> While a few momentum-dependent studies have been performed, the incident photon energy dependence, or resonance profile, is usually shown only for a few selected points in the Brillouin zone.

In this paper we present a theory for RIXS for the copper  $K$ -edge and present exact diagonalizations of Hubbard clusters of edge-sharing copper oxide plaquettes shown in Fig. 1. We calculate both the RIXS spectrum and the resonance profile for several cluster geometries, and determine the nature of excitations accessible via light scattering. We pay specific attention to the intermediate core-hole and final excited-state wavefunctions of RIXS accessible states. We find good agreement with the results on edge-shared copper oxide systems, and confirm a number of previous excitation assignments.<sup>10,11,12</sup>

## II. MODEL AND METHOD

### A. RIXS process

The RIXS process consists in scattering an incident photon of energy  $\hbar\omega_I$  off a sample in the ground state  $|\psi_0\rangle$  having energy  $E_0$ . For  $K$ -edge RIXS, an electron

from the 1s copper-core is photoexcited into the Cu 4p-band, leaving behind a core hole. The strong Coulomb repulsion between the core hole and  $d_{x^2-y^2}$  holes on the same Cu atom reorganizes charge density, forming an intermediate state  $|\psi_{ci}\rangle$  of eigenenergy  $E_{ci}$ . The 4p electron resides in a rather extended wave-function and therefore interacts weakly with  $d$  and core states. We neglect its interaction hence providing us with a rather simple description of RIXS. The 4p electrons then enter into the problem as a spectator at energy  $\epsilon_{4p} = \hbar\omega_I - (E_{ci} - E_0)$  and the intensity will be proportional to the projected

4p-band density of states (DOS) at that energy. The incident polarization determines the necessary orbital projection. The 4p electron then recombines with the 1s core hole emitting a photon of energy  $\hbar\omega_F$ , leaving the system in the final state  $|\psi_f\rangle$  of eigenenergy  $E_F$  and a photon energy transfer  $\hbar\Omega = \hbar\omega_I - \hbar\omega_F$ . This leads to a simplification of the general expression given in Ref.4. In this approximation the spectrum will be given by the following relation and with the  $\hbar\omega_I$  dependence given by a convolution with the 4p band DOS :

$$I(\omega_I, \Omega = \omega_I - \omega_F) \propto \sum_f \left| \sum_i \sum_{4p} \frac{\langle \psi_f | \psi_{ci} \rangle \langle \psi_{ci} | \psi_0 \rangle}{E_{ci} + \epsilon_{4p-1s} - E_0 - \hbar\omega_I - i\Gamma_1} \right|^2 \times \delta(E_F - E_I - \hbar\Omega). \quad (1)$$

Here  $\epsilon_{4p-1s}$  represents the Cu 1s – 4p energy separation. For simplicity, in a first approach, we neglect specific 4p orientation and photon polarizations. The polarization dependence, as well as the related 4p orientation and the 4p projected DOS, will be discussed in the last part of Section III. The parameter  $\Gamma_1$  represents damping of the intermediate state due to fluorescence and Auger 1s decay, which we take as 1.0 eV. While this value determines the overall resonant enhancement, it does not affect the resolution of the energy-loss peaks in the spectrum. We broaden the delta function with a width 0.1eV to represent current instrument resolution. We note that in Eq.(1) the states  $|\psi_{ci}\rangle$  are identical to those in a core x-ray photoemission experiment.

The Hamiltonian describing the open boundary cluster shown in Fig. (1), with rotated  $x$  and  $y$  local-directions along the  $p$  orbitals, is given by  $\mathcal{H} = \sum_{\langle i,j \rangle, \sigma} \mathcal{H}_{ij\sigma}^K + \sum_i (\sum_{\sigma} \mathcal{H}_i^{\epsilon} + \mathcal{H}_i^U) + U_Q \sum_{\sigma, \sigma'} d_{0,\sigma}^{\dagger} d_{0,\sigma} [1 - s_{0,\sigma'}^{\dagger} s_{0,\sigma'}]$ , with

$$\begin{aligned} \mathcal{H}_{ij\sigma}^K &= t_{pd} P_{i,j} p_{i,\sigma}^{\dagger} d_{j,\sigma} + t_{pdz} P_{i,j}^z p_{i,\sigma}^{\dagger} d_{z,j,\sigma} \\ &\quad + t_{pp} P_{i,j} p_{i,\sigma}^{\dagger} p_{j,\sigma} + t'_{pp} p_{i,\sigma}^{\dagger} p_{j,\sigma} + h.c \\ \mathcal{H}_i^{\epsilon} &= \epsilon_p (p_{i\sigma}^{\dagger} p_{i,\sigma} + p_{i,\sigma}^{\dagger} p'_{i,\sigma}) + \epsilon_d d_{i,\sigma}^{\dagger} d_{i,\sigma} + \epsilon_{dz} d_{z i,\sigma}^{\dagger} d_{z i,\sigma} \\ \mathcal{H}_i^U &= U_{pp} p_{i,\uparrow}^{\dagger} p_{i,\uparrow} p_{i,\downarrow}^{\dagger} p_{i,\downarrow} + U_{pp} p_{i,\uparrow}^{\dagger} p'_{i,\uparrow} p_{i,\downarrow}^{\dagger} p'_{i,\downarrow} \\ &\quad + U_{dd} d_{i,\uparrow}^{\dagger} d_{i,\uparrow} d_{i,\downarrow}^{\dagger} d_{i,\downarrow} + U_{dd} d_{z i,\uparrow}^{\dagger} d_{z i,\uparrow} d_{z i,\downarrow}^{\dagger} d_{z i,\downarrow}. \end{aligned}$$

Here  $d_{i,\sigma}^{\dagger}, d_{z i,\sigma}^{\dagger}, p_{i,\sigma}^{\dagger}, p'_{i,\sigma}$  and  $d_{i,\sigma}, d_{z i,\sigma}, p_{i,\sigma}, p'_{i,\sigma}$  creates and annihilates a  $d_{x^2-y^2}$ ,  $d_{3z^2-r^2}$ , planar  $p$  or  $p'$  hole with spin  $\sigma$  at site  $i$ , respectively, and the sum runs over nearest neighbors. The hopping amplitude  $t_{pp}$  refers to the hopping between two nearest  $p_x$   $p_y$  orbitals, and  $t'_{pp}$  refers to the hopping between two nearest-neighbor  $p_{\alpha}$  oxygen orbitals, where  $\alpha = x, y$ . The overlap phase factors are chosen such that  $P_{i,j} = 1$  for neighbors in the  $\mathbf{x}, -\mathbf{y}$  direction, and -1 for  $-\mathbf{x}, \mathbf{y}$ . The oxygen phase factors are analogously defined as  $P'_{i,j} = 1$  for oxygens at

$\mathbf{x}, \mathbf{y}$  and  $-\mathbf{x}, -\mathbf{y}$ , and -1 for the other combinations. Here  $s_0^{\dagger}$  (resp.  $s_0$ ) creates (annihilates) a Cu<sub>1s</sub> core-electron, and  $U_Q$  is the core -  $d$  hole repulsion. For simplicity we neglect interactions involving the 4p photo-excited electron, such as the 4p – 3d Coulomb interactions. These include off-diagonal couplings between  $d$  states which may be important for singlet-triplet energy differences as well as providing pathways for symmetry-allowed  $d - d$  excitations. We also neglect exchange interactions involving the 1s core-hole, which are very small.

In what follows, we use a standard set of parameters [in eV]<sup>5</sup>:  $t_{pd} = 1.1, t_{pp} = 0.5, t'_{pp} = -0.538 \times t_{pp}, \epsilon_d = 0, \epsilon_{dz} = 1.7, \Delta = \epsilon_p - \epsilon_d = 3.5, U_{pp} = 6, U_{dd} = 8.8$ , and  $U_Q = 8$ . These parameters give a value for the copper magnetic exchange  $J = 0.14$  eV for corner-shared copper oxides, and 2.8 meV for edge-shared.

## B. Discussion of the method and comparison with previous works

We first perform full exact-diagonalization of the Hamiltonian without the core-hole, and then redo the calculation with the core-hole. Since the Hamiltonian conserves the total spin, we diagonalized in the  $S=1/2$  sector. From the eigenvalues and eigenvectors of the two steps, the RIXS spectrum for a given  $\hbar\omega_I$  is computed from Eq.(1).

As our calculations involve determining the eigenvector of each state used to construct the matrix elements involved in RIXS, we know the character of each excitation exactly and do not need to make a priori assumptions about which peak corresponds to which fundamental excitation. This allows us to make direct correspondence between RIXS and other core-level spectroscopic techniques, without any further assumptions.

This is quite different from the Lanczos method, which

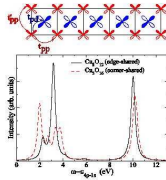


FIG. 1: Top: Edge-shared  $\text{Cu}_5\text{O}_{12}$  cluster. Bottom: XPS spectrum as a function of photon energy transfer and incident photon energy, for corner and edge-sharing copper-oxide clusters.

truncates the Hilbert space and focuses on the low-lying energy excitations. Whereas this method allows investigation of slightly larger clusters, extensions to higher energies is problematic particularly for RIXS where eigenvectors are needed to evaluate the matrix elements between higher energy states in order to obtain both the resonance profile (dependence on incident photon energies) as well as the intensities of prominent peaks in the spectrum. Since the core-hole interaction is essentially in nature (on-site Coulomb repulsion), leading to only a slight delocalization of the charge, we checked that the cluster-size does not play a crucial role in the qualitative shape of the spectra. In that sense, the calculations done in the present paper add more information and provide a more direct access to the relevant RIXS excitations compared to other techniques used in previous studies in the context of standard cuprates.<sup>14</sup> These studies treated the one-band Hubbard model where the Zhang-Rice singlets are, by construction, already formed, and focused only on the momentum dependence of the Mott gap excitation. By treating the problem in a multi-band model, the formation of Zhang-Rice excitations comes naturally in the problem and its signature in the RIXS intensity, peak dispersion and resonance profile can be directly addressed. In fact it is widely recognized that the gap is a charge transfer gap which involves transition from oxygen  $2p$  to copper  $3d$  states.<sup>15</sup>

### III. RESULTS AND DISCUSSIONS

#### A. Preliminary remarks

In core level x-ray photoelectron spectroscopy (XPS), the final state corresponds to an intermediate state in the RIXS process. We first plot the XPS spectrum for both edge-shared cluster  $\text{Cu}_5\text{O}_{12}$  and corner-shared cluster  $\text{Cu}_5\text{O}_{16}$  in Fig. (1). In both cases, the prominent features correspond largely to 1) a non-locally screened d-inter-site ZRS ( $d^9L$ ) feature at 2.2 eV, where the core hole has pushed a  $d^9$  hole from the on-site Cu onto the oxygen ligands in the neighboring plaquette, 2) a local

charge transfer (CT) excitation ( $d^{10}L$ ) at 3.5 eV whereby the screening of the core hole comes from the hole transfer from copper to oxygen on the same plaquette,<sup>16</sup> and 3) a 10 eV high-energy poorly screened  $d^9$  Cu hole on the core-hole site. These results are quantitatively similar to those presented earlier,<sup>17</sup> apart from a more realistic value of the exchange  $J$  in the corner-shared geometry. We note that x-ray absorption spectra in an extended system can be obtained from our XPS spectrum via a convolution with the copper  $4p$  DOS, giving a broad absorption edge followed by spectral intensity extending higher in energy governed by the  $4p$  bandwidth.

These excitations, present in both corner and edge-shared geometries, occur at roughly the same energy since they are governed by charge transfer energies and the exchange  $\propto t_{pd}^2/\Delta$  between copper and oxygen: the Cu-Cu exchange does not play a major role in setting these energy scales.

The main difference concerns the prominence of the non-locally screened d-inter-site ZRS excitation in the corner-shared compared with the edge-shared systems. While the ZRS accounts for nearly 80 percent of the ground state wavefunction including the core hole for the corner-shared plaquettes, it is approximately 56 % for the edge-shared system, reflecting the number of oxygen hybridization pathways available in the edge-shared configuration.<sup>18</sup> Thus while the energy is comparable in both systems, the matrix elements are much weaker at the ZRS scale in the edge-shared compared to corner-shared systems. In addition, the mobility of the ZRS for each geometry determines the peak widths, reflecting the splitting between bonding and anti-bonding ZRS on sites neighboring the core hole. In the case of the corner-shared systems, this corresponds to  $2t = -0.7\text{eV}$ , while due to the orientation of the orbitals in the edge-shared systems, the splitting is  $2t' = 0.3\text{eV}$ . As a result, the locally screened  $d^{10}L$  peak at 3.1 eV is much larger in edge-shared compared to corner-shared. This has led the phenomenon of high-temperature superconductivity, occurring in corner-shared compounds and absent in edge-shared compounds, to be associated with the stability of the ZRS.<sup>19</sup> We note that the primary role of the oxygen orientation in the formation of the ZRS is not captured in single-band Hubbard model calculations.

#### B. RIXS results : Attribution of the peaks

The aim of this subsection is to discuss the overall shape of the RIXS spectrum and resonant profile for a  $\text{Cu}_3\text{O}_8$  cluster in the inset of Fig. 2a. We show how to attribute to each peak the corresponding excitation, as an example, we have chosen the same parameters as for XPS in Fig. 1, appropriate for  $\text{Li}_2\text{CuO}_2$ . From here on we set  $\hbar$  equal to 1. Here the intermediate state core-hole is included on the edge of the cluster. The calculations are also performed for different locations of the core hole on the cluster, which has one hole per copper-plaquette.

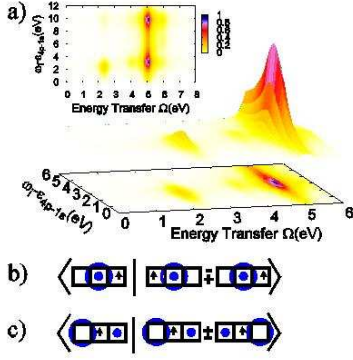


FIG. 2: a) RIXS spectra for  $\text{Cu}_3\text{O}_8$  cluster as a function of photon energy transfer  $\Omega$  and incident photon energy  $\omega_I$ , measured relative to the binding energy  $\epsilon_{4p-1s}$ . The inset shows a contour map over large frequencies. Matrix elements for  $\text{Cu}_3\text{O}_8$  are shown in b) & c), for the main peaks in RIXS at  $(\omega_i - \epsilon_{4p-1s}, \Omega) = (2.2, 2.2)$  and  $(3.1, 5.07)$ , eV respectively. Here the left, right eigenvector is the core hole, final state, respectively, and the dot and the circle represent a singlet state formed by a hole on the copper site (dot) and a hole delocalized on the oxygens having the ZR symmetry (circle).

While the results differ slightly for different locations of the core hole, we note that the changes are only quantitative and give different broadening of the RIXS peaks due to the different mobility of the d-intersite Zhang-Rice excitation on the end or middle of the cluster. However, since the aim of this paper is to compare trends for different cluster geometries and charge transfer energies, we will not discuss further these relatively minor changes in the spectra.

The RIXS spectrum shown in the inset of Fig. 2a consists of two prominent excitations at approximately  $\Omega = 5.07$  eV energy transfer, at incident photon energies of 3.1 and 10 eV. This is the local CT excitation, resonant at both the locally screened  $d^{10}L$  CT and poorly screened  $d^9$  intermediate states, as shown in Fig. 1. In addition a weaker d-intersite ZRS-derived peak is present at  $\Omega = 2.2$  eV, resonant for incident photon energies near 2.2 eV above the  $1s - 4p$  transition. The XPS spectra may be crudely viewed as a sum over all Raman shifts of the RIXS spectrum as a function of the incident photon energy  $\hbar\omega_I$ .

In Fig. 2a we show a blow up of the low energy RIXS spectrum. By examining the symmetries of the core-hole and final state wavefunctions, the nature of the RIXS excitations, and the origin of their resonant profile, can be determined by inspection of matrix elements appearing in Eq. 1. The ground state without the core hole  $|\psi_0\rangle$  is largely of  $d^9$  character in each plaquette. Only those intermediate states which have a large overlap with the ground state are relevant to the RIXS process. To deter-

mine which final states  $|\psi_{i \neq 0}\rangle$  are probed by RIXS and at what resonant energy they occur, one inspects the overlap of the core hole states  $|\psi_c\rangle$  reachable via the ground state without the core hole  $|\psi_0\rangle$ , with other excited states  $|\psi_{i \neq 0}\rangle$  in the same Hilbert space. For example, since the ground state of the cluster  $|\psi_0\rangle$  is a singlet, it cannot be coupled to triplet intermediate states having a core hole. We immediately conclude that for our cluster all triplet states do not appear in the RIXS process without spin-orbit coupling.

We sketch schematically in Fig. 2b and 2c the leading order contributions to the wave functions of the intermediate state with the core-hole and the final state with large matrix overlap, which correspond to the main excitations shown in the RIXS spectra. While the intermediate state is predominantly one configuration, the final states can either be bonding or anti-bonding combinations of excitations on the plaquettes, at energies approximately 2 eV above  $E_0$ , split by ZRS hopping.

In Fig. 2b, it is clear that the resonance peak at  $\omega - \epsilon_{4p-1s} = 2.2\text{eV}$  and energy transfer  $\Omega = 2.2\text{eV}$  comes from the combination of intermediate and final states corresponding to the creation of the ZRS in the final state, having strong overlap with the non-local, well-screened  $d^9L$  intermediate state. The two final states of bonding and anti-bonding combinations of ZRS on the two plaquettes couple to the intermediate state, with a weak splitting in edge-shared systems. Even with our broadening of 0.1eV the separate peaks are difficult to resolve.

The final states of the higher energy peak correspond to bonding and anti-bonding combinations of  $d^{10}L$ , having strong overlap with the intermediate core hole state with the ligand on the core hole site as shown in Fig. 2c. This lies at higher energy  $\omega_i - \epsilon_{4p-1s} = 3.07\text{eV}$ , and is the most prominent final state in XPS shown in Fig. 1.

We note that we do not find any prominent  $d-d$  excitations lying in the relevant energy range below 2 eV, even when including other  $d$  orbitals.<sup>20</sup> This follows from a symmetry analysis of the states, whereby  $d^9L$  and  $d^{10}L$  configurations cannot hybridize other Cu  $d$  orbitals and combinations of oxygen ligands. Thus direct  $d-d$  excitations are inaccessible in our model, in agreement with electron energy loss cluster calculations.<sup>21</sup> It is plausible that  $d-d$  excitations may arise if symmetry-breaking interactions with the 4p are included. This is different for oxygen 1s RIXS, as the creation of the core hole breaks this symmetry, allowing direct  $d-d$  excitations, as determined in recent cluster calculations.<sup>22</sup> Moreover,  $d-d$  excitations may arise from multiple couplings in non-resonant scattering<sup>23</sup> which are not treated in our calculation.

### C. Influence of the 4p-States – Polarization dependence – Material dependence

So far, our analysis did not include the copper-4p states. However, in order to obtain results more closely



connected to experiment and to include a photon polarization dependence for the Cu  $K$ -edge process, the Cu-4p DOS must be included into the calculations. Indeed, the Cu-1s core-electron can only be excited into the 4p-levels if there is a finite DOS for unoccupied states. Due to crystal field effects, the 4p DOS for different  $4p_{x,y,z}$  orbitals provide a polarization dependent shift of the resonance energies and secondary satellites governed by the peaks of each 4p projected DOS as well as the overall bandwidth. The orientation of the incident and emitted photon polarizations determine which 4p projected DOS is accessed.

Since the 4p-states are rather extended orbitals their interaction with the Hubbard subbands is quite weak. However, depending on the incoming light-polarization, matrix elements are selected so that one can access different linear combinations of  $4p_x$ ,  $4p_y$  and  $4p_z$  states. Since the DOS distributions are different, the RIXS spectra reflect these characteristics. Thus to deduce the influence of the 4p-states, we neglect minor real-space variations of the combined cluster-4p wavefunction and compute the convolution of our raw-RIXS spectrum with the calculated 4p projected DOS  $N_{4p}(\epsilon_{4p})$ :

$$\begin{aligned}
 I(\omega_I, \Omega = \omega_I - \omega_F) &\propto \sum_f \left| \sum_i \int d\epsilon_{4p} N_{4p}(\epsilon_{4p}) \frac{\langle \psi_f | \psi_{ci} \rangle \langle \psi_{ci} | \psi_0 \rangle}{E_{ci} + \epsilon_{4p-1s} - E_0 - \hbar\omega_I - i\Gamma_1} \right|^2 \times \delta(E_F - E_I - \hbar\Omega), \\
 &= \sum_f \left| \int d\epsilon_{4p} N_{4p}(\epsilon_{4p}) M(\hbar\omega_I - \epsilon_{4p-1s}, f) \right|^2 \times \delta(E_F - E_I - \hbar\Omega), \\
 \text{where } M(\hbar\omega_I, f) &= \sum_i \frac{\langle \psi_f | \psi_{ci} \rangle \langle \psi_{ci} | \psi_0 \rangle}{E_{ci} - E_0 - \hbar\omega_I - i\Gamma_1}.
 \end{aligned} \tag{2}$$

The projected 4p DOS is calculated using linearized augmented plane wave method (LAPW) in a coordinate system consistent with experiment.<sup>24</sup> In the following subsection we present results for different edge-shared cuprates  $\text{Li}_2\text{CuO}_2$  and  $\text{CuGeO}_3$ .

### 1. $\text{Li}_2\text{CuO}_2$

For  $\text{Li}_2\text{CuO}_2$ , the 4p projected DOS is shown in Fig. 3(a). The  $4p_z$  DOS has two sharp peaks at roughly 17eV, with subdominant peaks as shoulders to the main peak. The resulting RIXS spectrum for  $z$  photon polarizations shown in Fig. 3(b) thus has a shifted d-intersite ZRS resonance at  $\epsilon_{4p} - \omega_i \sim 19\text{eV}$  instead of 2.2eV in Fig. 2, yet remains sharply peaked even though the  $4p_z$  bandwidth is over 20 eV wide. The  $d^{10}L$  CT and poorly screened excitation at  $\Omega \sim 5\text{eV}$  are likewise shifted to higher resonance frequencies.

The  $4p_x$  DOS in Fig. 3(a) has a double-peak structure, with a single sharp peak at 4 eV and a tightly structured set of peaks around 10 eV. The resulting RIXS spectrum for photon polarizations along the  $x$ -axis, given in Fig. 3(c), clearly shows two split resonances at  $\sim 6-7\text{eV}$  and  $\sim 13\text{eV}$ , a shift of the raw RIXS spectrum (Fig. 2) by the 4eV and 10eV  $4p_x$  DOS peaks. The difference in the relative intensities between Fig. 3(b) and Fig. 3(c) is due to the fact that the DOS for the  $p_z$  orbitals is more intense at its maximum than for the  $p_x$  orbital.

Fig. 4 displays a side-by-side comparison of the present theory and recent experimental data by Kim *et al.*<sup>8</sup> on

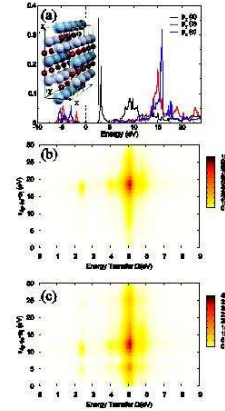


FIG. 3: (a) Cu-4p partial density of states for  $\text{Li}_2\text{CuO}_2$ . (b) RIXS spectrum for parameters corresponding to  $\text{Li}_2\text{CuO}_2$ , convoluted with the  $p_z$ -DOS. (c) RIXS spectrum for parameters corresponding to  $\text{Li}_2\text{CuO}_2$ , convoluted with the  $p_x$ -DOS. For both (b) and (c) we took a core-hole lifetime of  $\Gamma = 1.5\text{eV}$

$\text{Li}_2\text{CuO}_2$ . The theory and experimental curves show striking similarities in both the energy transfer and the incoming photon energy range. The energy scale, prominence of the local CT excitation, and the double resonance profile shown in Figs. 1,2,4 correspond well to the RIXS experiments. We remark that while Ref. 8 attributed the weak 2.1 eV peak to an interatomic  $d-d$

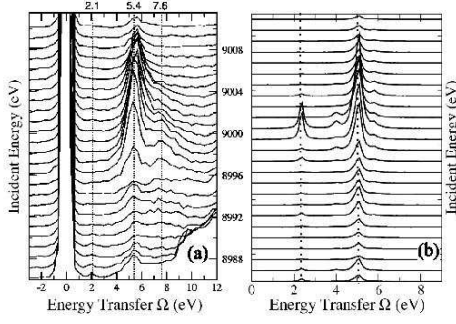


FIG. 4: (a) Experimental data for  $\text{Li}_2\text{CuO}_2$  by Kim *et al.* in Ref.8. (b) Calculated RIXS spectrum for parameters corresponding to  $\text{Li}_2\text{CuO}_2$  convoluted with the  $4p$ -DOS.

excitation, and the strong peak at 5.4 eV peak to local CT excitation, in view of our results we would conclude that the low energy excitation rather corresponds to the d-intersite ZRS excitation. The weak peak observed at 7.6 eV however has no correspondance in our calculations. This peak may be associated with a local CT excitation into states with different ligand symmetry orthogonal to the ZRS ligand states, which may become accessible once oxygen  $4p - 2p$  interactions are included.

## 2. $\text{CuGeO}_3$

As pointed out in Ref.6, the large valency of  $\text{Ge}^{4+}$  nearby the  $\text{CuO}$  planes increases the Madelung energy difference between the Cu and planar O sites in  $\text{CuGeO}_3$  compared to  $\text{LiCuO}_2$ , leading to the values  $\Delta = 4.9$  and 3.2 eV, respectively, for each system. Since this energy scale largely determines the energies of the d-intersite ZRS and the separation in energy to the local CT excitation, the RIXS spectrum and resonance profile should be largely different in the two cases.

In a first approach, as we did for  $\text{Li}_2\text{CuO}_2$ , we present in Fig. 5 a non-convoluted RIXS spectrum for parameters corresponding to  $\text{CuGeO}_3$ , which are the same set of parameters as before apart from the change  $t_{pd}=1.23$  eV, and  $\Delta = 4.9$  eV. The larger value of  $\Delta$  leads to several changes compared to the RIXS spectrum for  $\text{Li}_2\text{CuO}_2$  parameters (see Fig. 2.a). First, we note that the d-intersite ZRS peak has moved higher in energy from the  $d^9$  and core-hole ground states, lying at a photon energy transfer  $\Omega$  of 3.1 eV, and resonant at a higher incident photon energy  $\omega_i - \epsilon_{4p-1s} = 3.1$  eV. The bonding- antibonding splitting is smaller and the resonant peaks are more sharp. In addition, the CT ( $d^{10}L$ ) excitations move higher in energy, lying at  $\omega_i - \epsilon_{4p-1s} = 3.9$  eV and  $\Omega = 6.2$

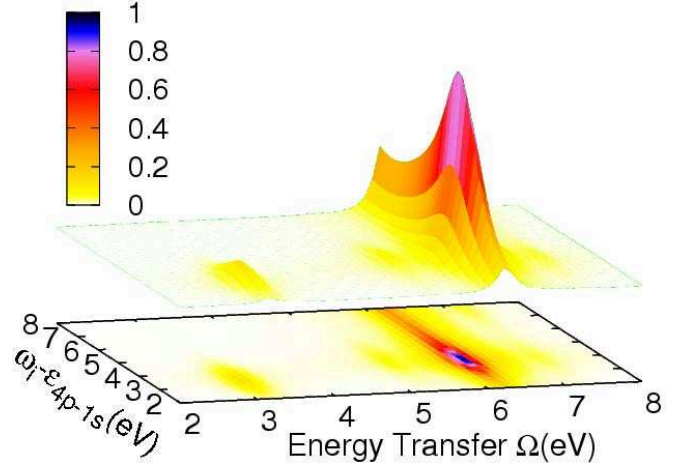


FIG. 5: RIXS spectrum as a function of photon energy transfer and incident photon energy for parameters corresponding to  $\text{CuGeO}_3$ , as defined in the text.

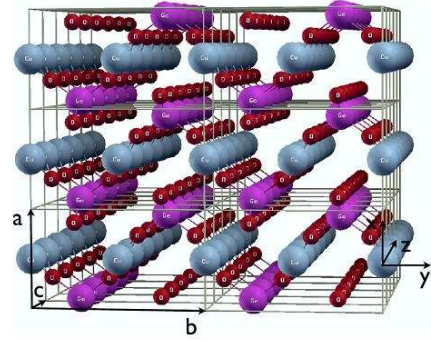


FIG. 6:  $\text{CuGeO}_3$  structure.

eV. This energy cost arises from the higher oxygen site energies as well as the reduction in exchange energy gain with the Cu spin.

The  $\text{CuGeO}_3$  structure in Fig.6 is different from the one of  $\text{Li}_2\text{CuO}_2$ : the copper chains run now along the  $c$ -direction and they are tilted from the main-axis planes. We present in Fig. 7(a) the  $4p$  projected DOS for  $\text{CuGeO}_3$ . The coordinates system for which the calculation has been done corresponds to the one presented in Fig.6. As one can see, the result is strongly dependent on polarization: the density of  $4p_y$  is peaked around  $\sim 8$  eV, the  $4p_z$ -density has its stronger weight around  $\sim 18$  eV and is much broader.

The corresponding RIXS results are shown for photon polarizations along  $p_y$  and  $p_z$  in Fig. 7(b) and (c), respectively. The overall shape of the spectra does not change much compared to the unconvoluted results (see Fig. 5) : one can still identify clearly a low-energy Zhang-

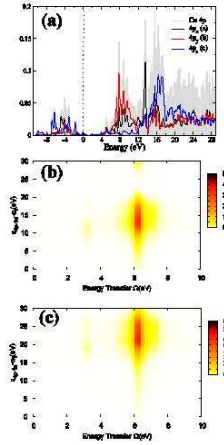


FIG. 7: (a) Cu-4p partial density of states in CuGeO<sub>3</sub> calculated in WIEN2k. (b) RIXS spectrum for parameters corresponding to CuGeO<sub>3</sub>, convoluted with the  $p_y$ -DOS. (c) RIXS spectrum for parameters corresponding to CuGeO<sub>3</sub>, convoluted with the  $p_z$ -DOS.

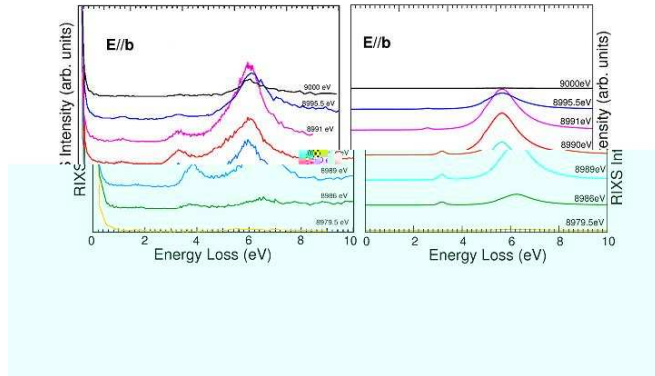


FIG. 8: (Left) Experimental RIXS spectrum for CuGeO<sub>3</sub>. (Right) Theoretical spectrum obtained for the same polarization.

Rice peak and a brighter  $d^{10}L$  peak at higher energy as well as the poorly screened  $d^9$  excitation peak. The main difference is a shift on the incident photon energy axis, of  $\sim 12$  eV for  $p_y$  and  $\sim 21$  eV for  $p_z$ .

These results are compared to the recent experimental spectrum obtained by Hill *et al.*<sup>25</sup> in Fig. 8 and 9. In this experiment a CT ( $d^{10}L$ ) peak at  $\Omega \approx 6.5$  eV and the ZRS peak as well, closer to the elastic line, at about  $\sim 3.8$  eV, were identified. These two observed peaks correspond to the two peaks seen in Fig. 5.

In Fig. 8 we have used an energy-dependent damping for the Lorentzian representing the delta function of Eq.(1). This energy dependence of the line width accounts for the fact that the higher energy states lie in

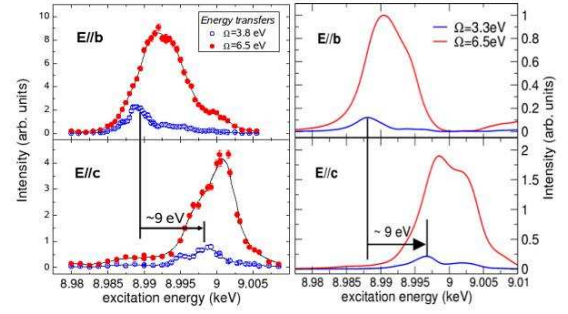


FIG. 9: (Left) Experimental RIXS spectrum for CuGeO<sub>3</sub> with polarization dependence. (Right) Exact-diagonalization results after convolution with the 4p projected DOS of Fig.7.(a) (see Subsection III C)

a high density continua. For  $\hbar\Omega < 5.5$  eV, a quadratic energy dependence of the damping rate was taken and assumed to saturate at higher Raman shifts. This form was chosen in order to account for the relative intensity and width of the ZR and  $d^{10}L$  peaks.

We note that the slight discrepancy between theory and experiment in the position and intensity of the d-intersite ZRS may be remedied by fine-tuning the cluster parameters, to more accurately reflect the material properties (such as  $J$  and the effective ZR-hopping  $t$ ), as well as incorporating a more realistic resolution broadening parameter. Another difference between theory and experiment is the relative intensity of the peaks for different polarizations: while the peaks are more intense for a polarization along **b** in the experiment, it is the opposite for the simulation. This issue may be related to the two following points: (i) from a theoretical point of view the relative intensity of the peaks is sensitively linked to the relative peaks height of the DOS (since in Eq.(1) it appears to be squared), thus a slight variation in the DFT calculation might make a difference. (ii) Due to experimental uncertainties a direct comparison of the measured absolute intensities for **e**||**b** and **e**||**c** is not possible. However, for a fixed polarization the measured relative intensities of the ZR and the CT feature can be compared.

Finally we remark that the crystal structures of CuGeO<sub>3</sub> and Li<sub>2</sub>CuO<sub>2</sub> are strongly different (see for instance Refs. 26,27). In both cases the CuO<sub>2</sub> chains run along a principal axis of the crystal but in CuGeO<sub>3</sub> they are not oriented along the same plane, whereas for Li<sub>2</sub>CuO<sub>2</sub> they are. This has strong implications concerning the interpretation of the experimental results : for CuGeO<sub>3</sub> the polarization-dependent experiments will give RIXS spectra which are a result of convolution with

the projected DOS in a rotated basis. The result of such a convolution is given in the right panel of Fig.9.

#### IV. CONCLUSIONS

A full exact-diagonalization treatment of multi-band Hubbard clusters has been used to calculate the polarization, incident photon energy, and transferred photon energy dependencies, of RIXS in one-dimensional, edge-shared insulating cuprates. By building upon previous work,<sup>16</sup> the RIXS spectrum can be constructed using XPS final-states as the intermediate states of inelastic x-ray scattering. The intensity and resonance profile, as well as the identity and character of the main RIXS peaks has been obtained using the eigenstates and eigenenergies of clusters with and without the core-hole. These peaks correspond to non-locally screened d-intersite ZRS  $d^9L$ , local CT  $d^{10}L$ , and poorly screened  $d^9$ , each having intensities and resonance profile determined by the overlap of these states with the intermediate core-hole states.

The polarization dependent RIXS spectra were obtained by convolving the raw RIXS spectra with the copper  $4p$  projected DOS determined by WIEN2k density functional calculations. While the resulting RIXS spectra includes the  $4p$  states as merely spectators to the re-arrangement of copper-oxygen valence charge density, a polarization and material dependent RIXS emerges due to the peak structures and intensities of the  $4p$  orbitally-projected intermediate states.

Direct comparison (see Figs. 4,9) with recent data for two edge-shared cuprates,  $\text{Li}_2\text{CuO}_2$  and  $\text{CuGeO}_3$ ,<sup>8,9,10,11,12</sup> shows both qualitative and, more importantly, quantitative agreements between theory and experiment for the shape, energy, width, and resonance profile of RIXS spectral features. This indicates that the local cluster model can adequately reproduce the data for photon energy losses in the energy range of 2-7 eV. We again remark that  $d-d$  excitations are not captured in the model, and further, that spin-flip excitations, which require large clusters to observe bi-magnon spin rearrangements at long wavelengths, are also very weak. Better agreement of the calculated spectra with

experiment may be obtained by using more refined cluster parameters, multi-pole couplings, and more accurate representation of resolution broadening.

A polarization dependent RIXS experimental study, for  $\text{Li}_2\text{CuO}_2$ , should find significant differences in the resonant profiles for in-plane polarization and polarization perpendicular to the  $\text{CuO}_2$ -plane. Fig. 3 indicates that peak intensities are brighter and their resonance energies are shifted by  $\sim 10$  eV for in-plane compared to perpendicular polarizations. These predictions as well as others, like multiple resonant features resulting from  $4p$ -projected states, open a way to infer from Cu  $K$ -edge and other indirect RIXS experiments the unoccupied DOS. In this way RIXS can be seen as a complementary tool to core-level spectroscopies such as XPS and XAS, providing at the same time diverse and important spectral information on elementary excitations in strongly correlated materials.

In summary, we have explored the Cu  $K$ -edge spectrum for different edge-shared copper oxide systems, and have shown that the energy scales, peak intensities, and resonance profiles can be explained qualitatively within the context of exact diagonalization studies of the multi-band Hubbard model. The prospect of mapping out the full momentum, and resonance profile dependences would allow for a direct spectral check of the many roles played by local electronic correlations in the multi-band Hubbard approach. This remains a topic of future research.

#### Acknowledgments

The authors wish to thank J. P. Hill, Y.-J. Kim, Z.-X. Shen, Z. Hussain, M. Z. Hasan, M. Greven, J. Hancock, and M. Gingras for many useful discussions. TPD and GAS would like to acknowledge support of this work in part by NSERC, CFI, ONR Grant N00014-05-1-0127 (TPD), PREA (TPD), the Alexander von Humboldt Foundation (TPD) and CIFAR (GAS). JG gratefully acknowledges the financial support by the DFG. TPD wishes to thank the Pacific Institute for Theoretical Physics for their hospitality. FV would like to thank financial support from CIFAR.

<sup>1</sup> A. Damascelli, Z. Hussain, and Z.-X. Shen, Rev. Mod. Phys. **75**, 473 (2003).

<sup>2</sup> J. Graf, G.-H. Gweon, A. Lanzara, cond-mat/0610313; J. Graf, G.-H. Gweon, K. McElroy, S. Y. Zhou, C. Jozwiak, E. Rotenberg, A. Bill, T. Sasagawa, H. Eisaki, S. Uchida, H. Takagi, D.-H. Lee, A. Lanzara, Phys. Rev. Lett. **98**, 067004 (2007); T. Valla, T. E. Kidd, Z.-H. Pan, A. V. Fedorov, W.-G. Yin, G.D. Gu, P.D. Johnson, cond-mat/0610249; B. P. Xie, K. Yang, D. W. Shen, J. F. Zhao, H. W. Ou, J. Wei, S. Y. Gu, M. Arita, S. Qiao, H. Namatame, M. Taniguchi, N. Kaneko, H. Eisaki, Z. Q. Yang, D.L. Feng, Phys. Rev. Lett. **98**, 147001 (2007); W.

Meevasana, X.J. Zhou, S. Sahrakorpi, W.S. Lee, W.L. Yang, K. Tanaka, N. Mannella, T. Yoshida, D. H. Lu, Y.L. Chen, R.H. He, Hsin Lin, S. Komiya, Y. Ando, F. Zhou, W.X. Ti, J.W. Xiong, Z. X. Zhao, T. Sasagawa, T. Kakeshita, K. Fujita, S. Uchida, H. Eisaki, A. Fujimori, Z. Hussain, R. S. Markiewicz, A. Bansil, N. Nagaosa, J. Zaanen, T.P. Devereaux, Z.-X. Shen, Phys. Rev. B **75**, 174506 (2007)

<sup>3</sup> T. P. Devereaux and R. Hackl, Rev. Mod. Phys. **79**, 175 (2007).

<sup>4</sup> P. M. Platzmann and E. D. Isaacs, Phys. Rev. B **57**, 11107 (1998); A. Kotani and Shin, Rev. Mod. Phys. **73**, 203



- (2001).
- <sup>5</sup> F. C. Zhang and T. M. Rice, Phys. Rev. B **37**, 3759 (1988); H. Eskes and G. A. Sawatzky, Phys. Rev. Lett. **61**, 1415 (1988); H. Eskes, L. H. Tjeng, and G. A. Sawatzky, Phys. Rev. B **41**, 288 (1990); H. Eskes and G. A. Sawatzky, Phys. Rev. B **44**, 9656 (1991).
  - <sup>6</sup> Y. Mizuno, T. Tohyama, S. Maekawa, T. Osafune, N. Motoyama, H. Eisaki, and S. Uchida, Phys. Rev. B **57**, 5326 (1998).
  - <sup>7</sup> J. B. Goodenough, Phys. Rev. **100**, 564 (1955); J. Kanamori, J. Phys. Chem. Solids **10**, 87 (1959); P. W. Anderson, Solid State Phys. **14**, 99 (1963).
  - <sup>8</sup> Young-June Kim, J. P. Hill, F. C. Chou, D. Casa, T. Gog, and C. T. Venkataraman, Phys. Rev. B **69**, 155105 (2004).
  - <sup>9</sup> D. Qian, Y. Li, M.Z. Hasan, D.M. Casa, T. Gog, Y.-D. Chuang, K. Tsutsui, T. Tohyama, S. Maekawa, H. Eisaki, and S. Uchida, J. Phys. Chem. Solids **66** 2212, (2005).
  - <sup>10</sup> M. Z. Hasan, Y.-D. Chuang, Y. Li, P. A. Montano, Z. Hussain, G. Dhaleenne, A. Revcolevschi, H. Eisaki, N. Motoyama, and S. Uchida, Int. Journ. Mod. Phys. B **17**, 3519 (2003).
  - <sup>11</sup> S. Suga, S. Imada, A. Higashiya, A. Shigemoto, S. Kasai, M. Sing, H. Fujiwara, A. Sekiyama, A. Yamasaki, C. Kim, T. Nomura, J. Igarashi, M. Yabashi, and T. Ishikawa, Phys. Rev. B **72**, 081101 (2005).
  - <sup>12</sup> M. v. Zimmermann, J. P. Hill, C.-C. Kao, T. Ruf, G.A. Sawatzky, T. Gog, C. Venkataraman, T. Masuda, I. Tsukada, and K. Uchinokura, preprint.
  - <sup>13</sup> L.-C. Duda, J. Downes, C. McGuinness, T. Schmitt, A. Augustsson, K. E. Smith, G. Dhaleenne, and A. Revcolevschi, Phys. Rev. B **61**, 4186 (2000).
  - <sup>14</sup> Kenji Tsutsui, Takami Tohyama, and Sadamichi Maekawa, Phys. Rev. Lett. **91**, 117001 (2003) ; K. Ishii, K. Tsutsui, Y. Endoh, T. Tohyama, S. Maekawa, M. Hoesch, K. Kuzushita, M. Tsubota, T. Inami, J. Mizuki, Y. Murakami, and K. Yamada, Phys. Rev. Lett. **94**, 207003 (2005).
  - <sup>15</sup> J. Zaanen, G. A. Sawatzky, and J. W. Allen, Phys. Rev. Lett. **55**, 418 (1985).
  - <sup>16</sup> M. A. van Veenendaal and G. A. Sawatzky, Phys. Rev. Lett. **70**, 2459 (1993).
  - <sup>17</sup> M. A. van Veenendaal, H. Eskes, and G. A. Sawatzky, Phys. Rev. B **47**, 11462 (1993); M. van Veenendaal **74**, 085118 (2006); K. Okada and A. Kotani, J. Phys. Soc. Japan, **75**, 044702 (2006).
  - <sup>18</sup> Due to the one-dimension geometry of the clusters, especially for the corner-shared case, the  $d^9L$  is not truly a ZRS as it has more weight on the central, bridging oxygen. However, the symmetry of this state remains ZR-like, maintaining the ZR signs of the ligands.
  - <sup>19</sup> Y. Ohta, T. Tohyama, and S. Maekawa, Phys. Rev. B **43**, 2968 (1991); C. Di Castro, L. F. Feiner, and M. Grilli, Phys. Rev. Lett. **66**, 3209 (1991); J. H. Jefferson, H. Eskes, and L. F. Feiner, Phys. Rev. B **45**, 7959 (1992); L. F. Feiner, M. Grilli, and C. Di Castro, Phys. Rev. B **45**, 10647 (1992); R. Raimondi, J. H. Jefferson, and L. F. Feiner, Phys. Rev. B **53**, 8774 (1996).
  - <sup>20</sup> C. de Graaf and R. Broer, Phys. Rev. B **62**, 702 (2000).
  - <sup>21</sup> S. Atzkern, M. Knupfer, M. S. Golden, J. Fink, A. Hubsch, C. Waidacher, K. W. Becker, M. Weiden and C. Geibel, Phys. Rev. B **64**, 075112 (2001).
  - <sup>22</sup> K. Okada and A. Kotani, Phys. Rev. B **63**, 045103 (2001).
  - <sup>23</sup> M. W. Haverkort, A. Tanaka, L. H. Tjeng, G. A. Sawatzky, cond-mat/arXiv:0705.4637 (2007).
  - <sup>24</sup> P. Blaha, K. Schwarz, G.K.H. Madsen, D. Kvasnicka, and J. Luitz, *WIEN2K, An Augmented Plane Wave + Local Orbitals Program for Calculating Crystal Properties*, ISBN 3-9501031-1-2 (TU Wien, Austria, 2001).
  - <sup>25</sup> J. Hill *et al.*, preprint
  - <sup>26</sup> M. Braden, G. Wilkendorf, J. Lorenzana, M. An, G. J. McIntyre, M. Behruzi, G. Heger, G. Dhaleenne, and A. Revcolevschi, Phys. Rev. B **54**, 1105 (1996).
  - <sup>27</sup> F. Sapiña, J. Rodriguez-Carvajal, M. J. Sanchis, R. Ibáñez, A. Beltrán, D. Beltrán, Solid State Comm. **74**, 779-784 (1990).